PHYSICAL REVIEW D VOLUME 35, NUMBER 2 15 JANUARY 1987

Inflation from inhomogeneous initial data in a one-dimensional back-reacting cosmology

Hannu Kurki-Suonio
Relativity Center, University of Texas, Austin, Texas 78712

Joan Centrella
Department of Physics and Atmospheric Science, Drexel University, Philadelphia, Pennsylvania 19104

Richard A. Matzner
Relativity Center, University of Texas, Austin, Texas 78712

James R. Wilson
Lawrence Livermore National Laboratories, Livermore, California 94550
(Received 3 September 1986)

We have simulated the onset of the inflationary era of the early Universe numerically, starting with inhomogeneous initial data for the Higgs field. Our computer code is fully general relativistic, including the gravitational effect of the Higgs field, and simulates a spacetime inhomogeneous in one space direction. According to our results, large initial fluctuations of the Higgs field do not prevent inflation, if the potential has the right shape. In a Coleman-Weinberg-type model with $\sigma=0.1m_{\rm Pl}$ inflation is realized for $\lambda\lesssim 10^{-2}$ and with $\sigma=0.01m_{\rm Pl}$ for $\lambda\lesssim 10^{-5}$.

I. INTRODUCTION

Advances in particle physics during the last decade have made it possible to study physical processes in the very early Universe; particle physics and cosmology have become important for each other. In this new cosmology one has to study the interplay between the new field theories and gravitation. The best examples of this are the old and new inflationary scenarios.[1] Because the main effect, exponential expansion of the Universe driven by the energy of the false vacuum, is gravitational, a proper treatment must be general relativistic.

In its original form the new inflationary scenario dealt with a spatially homogeneous situation. Recent criticism[2] has pointed out the importance of studying inhomogeneous situations. While homogeneous spacetimes can be treated by mainly analytical methods, numerical simulation is indispensable in studying inhomogeneous spacetimes with arbitrary initial conditions.

Numerical general relativity is one of the more difficult fields of computational physics. When the spacetime is filled with matter we have to do fluid dynamics simultaneously with the dynamics of the spacetime. Thus we have two interacting nonlinear theories. To this we now add a scalar field with its field equation, made nonlinear by a potential term.

We present fully general-relativistic numerical simulations of plane-symmetric cosmology. Our model spacetime is homogeneous in the x and y directions and inhomogeneous and periodic in the z direction. It is filled with a perfect fluid and a scalar field ϕ. This model is suitable for studying phase transitions of the early Universe. In a phase transition the scalar (Higgs) field makes a transition from a false vacuum to the true vacuum [global minimum of the potential $V(\phi)$]. We represent all matter other than the Higgs field as a perfect fluid with a radiation equation of state $p=\frac{1}{3}\rho$.

The physical situation addressed in this paper is the entrance to the inflationary era. We look for an unambiguous answer—for a range of parameters of the models—to the question: do initial inhomogeneities of the scalar field prevent inflation? As we shall see, for a range of parameters, these inhomogeneities do not prevent inflation.

The set of differential equations numerically integrated by our computer code is

$$\phi^{;\mu}{}_{;\mu}=dV(\phi)/d\phi\ , \tag{1.1}$$

$$T^{\mu\nu}_{(\rm fluid);\nu}=0\ , \tag{1.2}$$

$$G^{\mu\nu}=T^{\mu\nu}_{(\rm fluid)}+T^{\mu\nu}_{(\phi)}\ . \tag{1.3}$$

The scalar field equation (1.1) implies $T^{\mu\nu}_{(\phi);\nu}=0$. Thus we have separate conservation laws for the stress energy of the Higgs field and the fluid [Eq. (1.2)]. This means we are ignoring any coupling of the Higgs field to other fields. Such coupling would eventually be responsible for the reheating of the Universe at the end of the inflationary era. In such reheating the vacuum energy, which is then enormously larger than all other energies, is finally released, first into oscillations at the Higgs field [see, e.g., Figs. 7(d)—7(f)]. During the *onset* of new inflation, however, the gradients of the Higgs field are not relatively large, and the coupling is not essential for the description of the physical situation. In our model the Higgs field and the fluid do, of course, interact gravitationally.

$V(\phi)$ is the potential of the Higgs field. We study two different forms of the potential: a Coleman-Weinberg-[3] (CW) type potential, which is very flat close to the false vacuum, and a rounder ϕ^4-type potential. We do not include coupling to other fields. Such coupling is usually

cited as the source of temperature-dependent corrections which make $\phi=0$ a global minimum of the effective potential at high temperatures, but, however, Matzner[4] has shown that short-wavelength modes of ϕ itself actually play such a role in our model.

We use rationalized Planck units, where $8\pi G=\hbar=c=1$. (Unfortunately, the conventional Planck units are defined with $G=1$, resulting in differences of $\sqrt{8\pi}\simeq 5.0$.) Thus, we measure time in units of $1=5t_{\rm Pl}=2.7\times 10^{-43}$ s and the Higgs field in units of $1=0.2m_{\rm Pl}=2.4\times 10^{18}$ GeV.

Recently, Albrecht, Brandenberger, and Matzner[5] (ABM) studied the problem of realizing inflation starting from inhomogeneous initial conditions for ϕ. This work involved a numerical simulation of the behavior of the ϕ field in a homogeneously expanding background spacetime.

We have applied our code to the same problem. Instead of a homogeneous background spacetime as used by ABM, we accurately simulate a dynamical spacetime interacting with its scalar field and fluid content. Thus we will actually see an exponential expansion of space when inflation is realized.

Section II describes how we added a scalar field to the pre-existing plane-symmetric cosmological code of Centrella and Wilson.[6] Section III is on code tests. In Sec. IV we discuss the problem of inflationary and inhomogeneous initial conditions. Section V gives the results of our simulations.

II. THE DIFFERENTIAL EQUATIONS

The computer code used for the simulations here is based on the plane-symmetric Centrella-Wilson code described in Ref. 6. This code solves the equations of general relativity coupled to hydrodynamics. The matter content of the spacetime is represented by a one-component perfect fluid.

We have added to the code a scalar ("Higgs") field ϕ with a field equation

$$\phi^{;\mu}{}_{;\mu}=dV(\phi)/d\phi\ , \tag{2.1}$$

and a stress-energy tensor

$$T^{\mu\nu}_{(\phi)}=\partial^\mu\phi\partial^\nu\phi-[\tfrac{1}{2}\partial_\sigma\phi\partial^\sigma\phi+V(\phi)]g^{\mu\nu}\ , \tag{2.2}$$

where $V(\phi)$ is the potential for the field, including the term describing the mass of the ϕ field. Because of the covariant derivatives in (2.1) the behavior of this field is affected by the spacetime curvature. The energy-momentum tensor of the ϕ field contributes to the gravitational equations thereby affecting the curvature. For simplicity we do not include a direct coupling between the scalar field and the fluid (this will be treated in a later paper), so they interact only gravitationally.

We shall not here repeat the discussion of the differential equations of the Centrella-Wilson code (see Ref. 6), but focus on what has been added. The field equation (2.1) is spelled out as

$$\begin{aligned}\frac{1}{\sqrt{-g}}\partial_0[\sqrt{-g}\,g^{0\nu}\partial_\nu\phi+\partial_i(\sqrt{-g}\,g^{i0}\phi)]&\\ =-\frac{1}{\sqrt{-g}}\partial_i[\sqrt{-g}\,g^{ij}\partial_j\phi-\phi\partial_0(\sqrt{-g}\,g^{i0})]&\\ +dV(\phi)/d\phi\ .&\end{aligned} \tag{2.3}$$

Defining

$$\pi\equiv-\sqrt{-g}\,g^{0\nu}\partial_\nu\phi-\partial_i(\sqrt{-g}\,g^{i0}\phi)\ , \tag{2.4}$$

we get a pair of differential equations

$$\begin{aligned}\partial_t\phi&=\frac{-1}{\sqrt{-g}\,g^{00}}[\pi+\sqrt{-g}\,g^{0i}\partial_i\phi+\partial_i(\sqrt{-g}\,g^{i0}\phi)]\ ,\\ \partial_t\pi&=\partial_i[\sqrt{-g}\,g^{ij}\partial_j\phi-\phi\partial_t(\sqrt{-g}\,g^{i0})]-\sqrt{-g}\,V'(\phi)\ ,\end{aligned} \tag{2.5}$$

that are first order in time.

Specializing now to the plane-symmetric case, $\phi=\phi(z,t)$, and to the Centrella-Wilson form of the metric,

$$g_{\mu\nu}=\begin{bmatrix}-\alpha^2+A^2\beta^{x\,2}+A^2\beta^{z\,2} & A^2\beta^x & 0 & A^2\beta^z\\ A^2\beta^x & A^2 & 0 & 0\\ 0 & 0 & A^2h^2 & 0\\ A^2\beta^z & 0 & 0 & A^2\end{bmatrix}\ , \tag{2.6}$$

we get the equations of the scalar field used for our code:

$$\begin{aligned}\partial_t\phi&=\frac{\alpha}{\sqrt{\gamma}}\pi+2\beta^z\partial_z\phi\\ &\quad+\left[\frac{1}{\sqrt{\gamma}}\beta^z\partial_z\sqrt{\gamma}-\frac{1}{\alpha}\beta^z\partial_z\alpha+\partial_z\beta^z\right]\phi\ ,\\ \partial_t\pi&=\partial_z\left[\left[\left(\frac{1}{A^2}-\frac{\beta^{z\,2}}{\alpha^2}\right)\alpha\sqrt{\gamma}\partial_z\phi\right.\right.\\ &\quad\left.\left.-\left[\frac{\beta^z}{\alpha}\partial_t\sqrt{\gamma}+\sqrt{\gamma}\frac{\partial_t\beta^z}{\alpha}-\sqrt{\gamma}\frac{\beta^z}{\alpha^2}\partial_t\alpha\right]\phi\right]\right.\\ &\quad-\alpha\sqrt{\gamma}dV(\phi)/d\phi\ .\end{aligned} \tag{2.7}$$

For the time derivative of the determinant γ of the three-metric in the latter equation we use

$$\partial_t\sqrt{\gamma}=\beta^z\partial_z\sqrt{\gamma}-\alpha\sqrt{\gamma}(\tfrac{3}{2}\mathrm{tr}K-\tfrac{3}{2}K^z_z+\tfrac{1}{2}K_1)\ , \tag{2.8}$$

where the K_{ij} are components of the second fundamental form and $K_1\equiv K^x_x-K^y_y$ (see Ref. 6).

We must add the scalar field contribution to the gravitational source terms. These appear in the code in the forms

$$\begin{aligned}
&\rho_H \equiv n^\nu n^\delta T_{\nu\delta} ,\\
&S_\alpha \equiv -\gamma_\alpha^\nu n^\delta T_{\nu\delta} ,\\
&S_{\alpha\beta} \equiv \gamma_\alpha^\nu \gamma_\beta^\delta T_{\nu\delta} ,\\
&S \equiv S_\alpha^\alpha = \gamma_\alpha^\nu \gamma^{\delta\alpha} T_{\nu\delta} ,
\end{aligned} \tag{2.9}$$

where n is the normal to our spacelike three-slice,

$$n_\mu = (-\alpha,0,0,0) ,$$

and the three-metric is defined by

$$\gamma_{\mu\nu} = g_{\mu\nu} + n_\mu n_\nu ,$$

$$\gamma_{ij} = \mathrm{diag} A^2(1,h^2,1) .$$

For the scalar field we have

$$\begin{aligned}
&\rho_H^{(\phi)} = \frac{1}{2\alpha^2}(\partial_t\phi - \beta^z\partial_z\phi)^2 + \frac{1}{2A^2}(\partial_z\phi)^2 + V(\phi) ,\\
&S_x^{(\phi)} = 0 ,\\
&S_z^{(\phi)} = -\frac{1}{\alpha}(\partial_t\phi - \beta^z\partial_z\phi)\partial_z\phi ,\\
&S^{(\phi)} = \frac{3}{2\alpha^2}(\partial_t\phi - \beta_z\partial_z\phi)^2 - \frac{1}{2A^2}(\partial_z\phi)^2 - 3V(\phi) .
\end{aligned} \tag{2.10}$$

The source terms (2.9) appear in the Hamiltonian and momentum constraints, in the lapse equation and in the K_1 evolution equation. Of those, the x-momentum constraint and the K_1 equation are not affected when the scalar field is independent of x and y coordinates. The new Hamiltonian constraint equation is

$$\begin{aligned}
\partial_z(A^2\partial_z h) = h\Bigg[&-2A\partial_z\partial_z A + (\partial_z A)^2 - A^4\Bigg[-\tfrac{1}{4}(\mathrm{tr}K)^2 - \tfrac{1}{2}(\mathrm{tr}K)K_z^z + \tfrac{3}{4}(K_z^z)^2 + (K_x^z)^2 + \tfrac{1}{4}K_1{}^2\\
&+ \rho_H^{(\mathrm{fluid})} + \frac{1}{2\alpha^2}(\partial_t\phi - \beta^z\partial_z\phi)^2 + \frac{1}{2A^2}(\partial_z\phi)^2 + V(\phi)\Bigg]\Bigg] ,
\end{aligned} \tag{2.11}$$

where $\rho_H^{(\mathrm{fluid})}$ is the part of the Hamiltonian density due to the ordinary matter (see Ref. 6).

The new lapse equation is

$$\begin{aligned}
\partial_z(Ah\partial_z\alpha) - \alpha\sqrt{\gamma}\Bigg[&K_j^i K_j^i + \sigma(w^2 - \tfrac{1}{2}) + p\\
&+ \frac{1}{\alpha^2}(\partial_t\phi - \beta^z\partial_z\phi)^2 - V(\phi)\Bigg]\\
&+ \sqrt{\gamma}\partial_t(\mathrm{tr}K) = 0 ,
\end{aligned} \tag{2.12}$$

and the new z-momentum constraint is

$$\begin{aligned}
&\partial_z[A^3h^{3/2}(K_z^z - \tfrac{1}{3}\mathrm{tr}K)]\\
&\quad = A^3h^{3/2}\left[S_z - \frac{1}{\alpha}(\partial_t\phi - \beta^z\partial_z\phi)\partial_z\phi - \frac{1}{2}\frac{\partial_z h}{h}K_1\right] ,
\end{aligned} \tag{2.13}$$

where S_z refers to the momentum of the fluid only.

In each cycle the code calculates a new spacelike three-slice one time step further in time. The order of calculation within each cycle is (1) extrinsic curvature K_1, tr$K$, K_x^z, K_z^z, (2) shift vector β^x, β^z, (3) scalar field canonical conjugate π, (4) three-metric A, h (update D, E, S_x, S_z for volume), (5) scalar field ϕ, (6) hydrodynamical quantities D, E, S_x, S_z, (7) lapse function α, (8) recompute h from Hamiltonian constraint.

See Ref. 6 for quantities not defined here. As explained in Ref. 6 the inclusion of both the evolution equation of h and the Hamiltonian constraint gives one equation more than there are variables. Thus, the Hamiltonian constraint should be automatically satisfied after steps 1–7. In a numerical calculation there will always be a small error. In particular the accumulation of numerical errors makes the coefficients in the equation for h incompatible with periodicity. Therefore in the eighth step the variables are fine-tuned to satisfy the constraint. This improves the accuracy and stability of the code. To monitor the accuracy of the simulation, the code keeps count of the cumulative amount of fine-tuning done. Obviously any accuracy and stability problems will show up here. Since such problems appeared in some cases we discuss the treatment of the Hamiltonian constraint.

The Hamiltonian constraint can be viewed as a second-order differential equation for h, with periodicity of h and $\partial_z h$ as boundary conditions. We take the boundary values of h and $\partial_z h$ from step (4), and integrate across the slice. This is then repeated with adjusted boundary values until periodicity is achieved.

If we were to do this naively, we would immediately get into trouble, since the Hamiltonian constraint is a linear homogeneous differential equation for h. The coefficients in this equation define a function with a definite period, completely analogously to the definite period defined by the harmonic-oscillation equation. However, here we have the requirement that this period coincide with the length of our computational grid. In this form, if periodicity is not achieved with one boundary value for h, no amount of adjusting it will help.

Note that $\rho_H^{(\mathrm{fluid})}$ is a mass-energy density source. Therefore $\sqrt{\gamma}\rho_H^{(\mathrm{fluid})} \equiv A^3h\rho_H^{(\mathrm{fluid})}$ is an infinitesimal element of mass energy which should be conserved in general and in particular during the solution of this equation. This introduces an inhomogeneous term in the differential equation for h, and allows adjustment to find periodicity. Of course, once we have obtained the adjusted value of h we must rescale this term to account for this change. Hence, during the solution of the Hamiltonian constraint for h, the term $A^4h\rho_H^{(\mathrm{fluid})}$ will be held constant. Similarly the term $\frac{1}{4}A^4hK_1{}^2$ corresponds to gravity wave energy and is also to be conserved. The scalar field adds additional source terms to the Hamiltonian constraint which we also identify as conserved mass-energy terms.

With this prescription the Hamiltonian constraint appears in the form

$$\partial_z(A^2\partial_z h)=hX-L-D_1-\Psi-\theta\ , \tag{2.14}$$

where

$$X=(\partial_z A)^2-2A\partial_z{}^2A - A^4[(K_x^z)^2+\tfrac{3}{4}(K_z^z)^2-\tfrac{1}{2}(\mathrm{tr}K)K_z^z-\tfrac{1}{4}(\mathrm{tr}K)^2]\ ,$$

$$L=A^4h(\sigma w^2-p)\ ,$$
$$D_1=\tfrac{1}{4}A^4h(K_1)^2\ , \tag{2.15}$$
$$\Psi=A^4hV(\phi)\ ,$$

$$\theta=A^4h\left[\frac{1}{2\alpha^2}(\partial_t\phi-\beta^2\partial_z\phi)^2+\frac{1}{2A^2}(\partial_z\phi)^2\right]\ .$$

This is now an inhomogeneous equation for h with sources which are conserved, and an iteration scheme is possible.

This appears to work best when the fluid is the dominant source term. When other source terms dominate we used a more complicated scheme. In the preceding we have implicitly taken the view that if the constraint is not satisfied, the reason is that h is off and has to be fine-tuned. Of course we could as well adjust any of the quantities calculated in steps (1)–(7) and that are involved in the constraint. This opens up an infinity of different fine-tuning schemes. Since any adjusting violates the other equations, which produced the unadjusted values, we are justified only so far as the adjustments are small. The ideal thing would be to find the smallest possible adjustment which satisfies the constraint.

In the models we want to study, the potential $V(\phi)$ has a complicated nonlinear form and thus the ϕ contribution to the constraint equation changes irregularly under adjustment of ϕ. For any simple ϕ adjusting scheme, there are configurations for which a large adjustment produces only a small change in the total ϕ contribution. This may be the reason for the difficulties our code had with domain walls. We experimented with several nonlinear ϕ adjusting schemes, but settled on the following simple linear scheme.

For Eq. (2.14) to yield a periodic $\partial_z h$ we should have

$$S_1-S_2-S_3-S_4-S_5=0\ , \tag{2.16}$$

where

$$S_1=\oint hX\,dz\ ,$$
$$S_2=\oint L\,dz\ ,$$
$$S_3=\oint D_1\,dz\ , \tag{2.17}$$
$$S_4=\oint \Psi\,dz\ ,$$
$$S_5=\oint \theta\,dz\ .$$

We will adjust h, K_1, and ϕ to satisfy (2.16). To minimize unnecessary adjustments that lead to little improvement we weight the adjustments with the relative contribution to the source term. The new values will be

$$h^{\mathrm{new}}=(1+YS_2)h\ ,$$
$$K_1^{\mathrm{new}}=(1-YS_3)K_1\ , \tag{2.18}$$
$$\phi^{\mathrm{new}}=[1-Y(\tfrac{1}{2}S_d+S_5)]\phi\ ,$$

where S_d is the derivative of S_4 with respect to adjusting ϕ:

$$S_d=\oint hA^4\frac{dV}{d\phi}\phi\,dz\ . \tag{2.19}$$

The small parameter Y is determined from

$$S_1(1+YS_2)-S_2-S_3(1-YS_3)^2-S_4+Y(\tfrac{1}{2}S_d+S_5)S_d - S_5[1-Y(\tfrac{1}{2}S_d+S_5)]^2=0\ . \tag{2.20}$$

To first order in Y we get

$$Y=-\frac{S_1-S_2-S_3-S_4-S_5}{S_1S_2+2(S_3)^2+\frac{1}{2}(S_d+2S_5)^2}\ . \tag{2.21}$$

We then set $\phi=\phi^{\mathrm{new}}$, $K_1=K_1^{\mathrm{new}}$ and at the boundary $h=h^{\mathrm{new}}$. We solve h from (2.14) iterating on the boundary value of $\partial_z h$ until we get a solution periodic in h.

In a typical run, the cumulative adjustment done in the Hamiltonian constraint subroutine stays below 2% for many thousands of cycles, unless domain walls form. In the presence of domain walls the simulation soon becomes unstable, in some cases [Figs. 7(a) and 10(a)] immediately after the walls have formed, in other cases [Figs. 10(b) and 12] a few oscillation periods later. This is seen in the rapid growth of the adjustment of the ϕ field (sometimes h is affected too) and also in that the behavior of the simulation becomes irregular. In the figures we have cut out the final unreliable part, showing only the good part of the simulation when the adjustment is still small. We discuss this point further in the conclusion.

III. CODE TESTS

The geometry code, that is the code without the scalar field, has already been thoroughly tested by Centrella and Wilson.[6] Thus, it is only necessary to test the new contributions from the scalar field. (Several of those old tests were, however, repeated to ensure that no accidental damage had been done to the code during any step.)

To test the effect of the vacuum energy of the scalar field on the expansion we did a test run with Friedmann-Robertson-Walker (FRW), i.e., homogeneous, isotropic initial data. The model calculated had initial radiation energy density $\rho_{(\mathrm{fluid})}=\rho_0=6.58\times10^{-5}\ (0.2m_{\mathrm{Pl}})^{-2}$ and the scalar field constant, $\phi\equiv0$, with vacuum energy density $V=V(\phi=0)=0.2\times10^{-5}\times(0.2m_{\mathrm{Pl}})^{-2}$. (The specific numbers were chosen because they are typical of the inhomogeneous simulations of this paper.) The theoretical expansion of such a FRW spacetime containing radiation and vacuum energy is given by simple integration:

$$R^2(t)=R_0{}^2\left[\frac{\rho_0}{V}\right]^{1/2}\sinh\left[\frac{4V}{3}\right]^{1/2}t\ . \tag{3.1}$$

Figure 1 presents the results graphically and shows the inflating behavior of R. Notice that the scale in Fig. 1 and

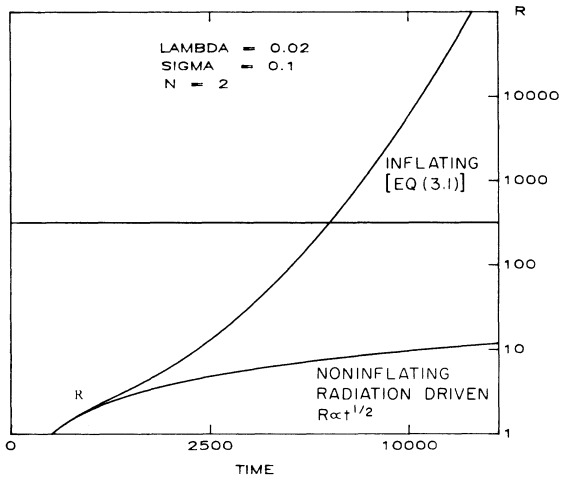

FIG. 1. Homogeneous cosmologies. We plot the expansion factor vs time for two cases: the inflating solution of Eq. (3.1), and a noninflationary model which is simply driven by radiation, with scale factor $R \propto t^{1/2}$. Notice that the horizontal (time) scale is linear in $t^{1/2}$; the vertical, R, scale is linear in the logarithm. This choice of scalings used here and in our subsequent plots of inhomogeneous models allows a wide range of behavior to be displayed.

the other figures in R is linear in the logarithm. The inflating behavior does not give a straight line, however, because the horizontal scale is linear in $t^{1/2}$. Similarly, the noninflating radiation driven solution does not show a straight line (R vs $t^{1/2}$); rather is the graph of the logarithm, since the vertical scale is logarithmic. This choice of scaling was found best able to handle the range of behavior of the inhomogeneous solutions. We compare in Table I the values of various quantities from an early and late stage of the test run to theoretical values. The agreement is very good over a factor $\sim 10^{10}$ in volume. In the table the volume is normalized so that the initial volume $=1$. K_1 (the metric anisotropy momentum) and D (the matter rest mass density) were essentially zero in this run. For those who wish further graphical results, we note that in Sec. V there are several models [Figs. 7(b), 7(c), 7(g)] that enter inflation and behave in an exponential way similar to Eq. (3.1).

TABLE I. A test run with vacuum energy.

Volume:	7.789	2.56×10^{11}
Quantity	Relative error	
A	<0.01	<0.01
h	0.01	0.01
K_1		
K_z^z	<0.01	<0.01
$\mathrm{tr}K$	<0.01	<0.01
D		
E	<0.01	0.01
A^3h	<0.01	0.01

Further tests can be carried out by considering situations where the scalar field produces simply a perturbation on a radiation-driven expanding cosmology. In particular, we did test runs with small oscillations of the scalar field around a minimum of the potential. If the location of the minimum of the potential is $\phi=\sigma$, then the potential can be approximated by

$$V(\phi)\simeq\tfrac{1}{2}\omega_0^2(\phi-\sigma)^2 . \tag{3.2}$$

In our test cases we had $\omega_0=0.04$. [We actually used the CW potential of Eq. (4.1) below with $\lambda=0.02$ and $\sigma=0.1$.]

In these runs the energy density is dominated by a homogeneous radiation fluid, so that the spacetime expands as $R\propto t^{1/2}$. The wavelength of a plane wave grows with the expansion, so that the wave number stays constant in comoving coordinates. Thus, a standing plane wave in the scalar field is given by $\phi(t,z)-\sigma=\psi(t)\sin qz$, where $\psi(t)$ satisfies the equation

$$\ddot{\psi}+\frac{3}{2t}\dot{\psi}+\left[\frac{q^2}{t}+\omega_0^2\right]\psi=0 , \tag{3.3}$$

where the overdot means ∂_t. All the geometrical variables are made initially homogeneous and all remained so consistently during the evolutions.

We first test the case of a homogeneous scalar field, i.e., $q=0$, for which Eq. (3.3) becomes

$$\ddot{\psi}+\frac{3}{2t}\dot{\psi}+\omega_0^2\psi=0 . \tag{3.4}$$

We set initially $\psi=10^{-6}$. The solutions of Eq. (3.4) are

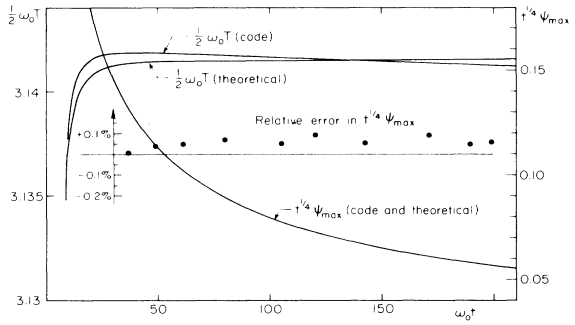

FIG. 2. Comparison of the test results with theoretical values for small oscillations of a homogeneous scalar field. The comparison is done separately for the amplitude $\psi_{\max}$ (maximum absolute value reached in a period) and the period T. The theoretical behavior is $\psi\propto t^{-1/4}J_{1/4}(\omega_0 t)$, so we compare $t^{1/4}\psi_{\max}$ to the maxima of $J_{1/4}(\omega_0 t)$. (The values of $\psi_{\max}$ have been rescaled to make the two values equal at approximately $\omega_0 t=30$.) In the scale of the figure the difference cannot be seen, so we have plotted the relative error on a separate scale. The error stays below 0.1%, which is very satisfactory. We also show the half periods $T/2$ (distance between successive zeros) of $\psi(t)$ from the test run and from $J_{1/4}(\omega_0 t)$. The theoretical values rapidly approach π/ω_0. Since all values lie so close, we again had to use a very fine scale to expose the small difference. See Eqs. (3.2)—(3.5).

Bessel functions of order $\frac{1}{4}$:

$$\psi(t)=t^{-1/4}[AJ_{1/4}(\omega_0 t)+BJ_{-1/4}(\omega_0 t)] . \quad (3.5)$$

The comparison between the test results and this theoretical behavior was done by comparing separately the amplitude and the period of the oscillations (see Fig. 2, noting especially the greatly expanded vertical scale. The agreement is very good indeed).

Next we tested the case of a plane wave with a wavelength equal to the size of our grid. Our choice of initial values corresponds to $q=1.033$. For this case we did not have an analytic solution of (3.3). The behavior of the amplitude and frequency of $\psi(t)$ can be seen easily, however.

At early times the term q^2/t dominates over ω_0^2. If ω_0^2 is ignored, the solutions are

$$\psi(t)=A'j_0(2qt^{1/2})+B'n_0(2qt^{1/2})$$
$$=t^{-1/2}(A\sin 2qt^{1/2}+B\cos 2qt^{1/2}) , \quad (3.6)$$

with amplitude $\propto t^{-1/2}$ and angular frequency $\sim q/t^{1/2}$. At larger times the solution approaches (3.5) with amplitude $\propto t^{-3/4}$ and angular frequency ω_0. As can be seen in Fig. 3(a) the code does indeed produce this behavior of the amplitude. The change from $t^{-1/2}$ to $t^{-3/4}$ behavior occurs smoothly when the terms ω_0^2 and q^2/t are comparable.

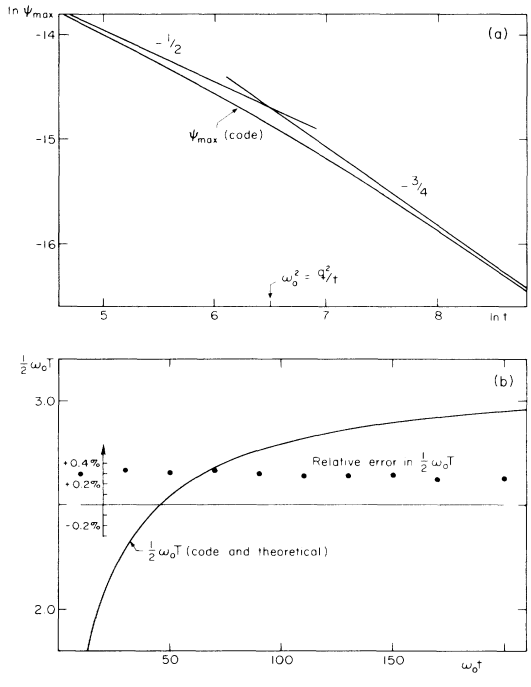

FIG. 3. Comparison of the test results with theoretical values for small oscillations of an inhomogeneous scalar field. (a) A log-log plot of the amplitude ψ_{max} vs time shows that the amplitude has the correct behavior: $\propto t^{-1/2}$ at small times and $\propto t^{-3/4}$ at large times. (b) The curve shows the half period $\frac{1}{2}\omega_0 T$ as a function of time as obtained from the test simulation. In this scale it is indistinguishable from the theoretical value $\pi/(1+q^2/\omega_0^2 t)^{1/2}$, so we plot the relative error on a separate scale. The error stays below 0.4% which is quite satisfactory. See Eq. (3.6).

The angular frequency is given very accurately by $(\omega_0^2+q^2/t)^{1/2}$ except at the very earliest times. The comparison of the test results to this is presented in Fig. 3(b).

These code tests focus on the aspects of the code most important for the simulations used for the results in this paper. The good accuracy demonstrated leaves us confident that the code behaves reliably in these simulations.

As another check we ran the code with the gravitational effect of the scalar field turned off, and were then able to duplicate the results of ABM. This is discussed in Sec. IV (Fig. 12).

IV. INHOMOGENEOUS INITIAL CONDITIONS

The standard inflationary model has been criticized by Mazenko, Unruh, and Wald.[2] They argue that at high temperatures in the early Universe the Higgs field ϕ would have large fluctuations as a function of space, and thus effective-potential methods which are based on a homogeneous expectation value of ϕ are not justified. Because of those fluctuations ϕ would initially have values close to the true vacuum at some regions of space. These regions would be trapped in the true vacuum already at the critical temperature. Thus, instead of a slow rolling of the expectation value $\langle\phi\rangle$ down from the false vacuum, we would get immediate domain formation and no inflation.

Motivated by this, ABM (Ref. 5) studied the problem of realizing inflation from "quasithermal" initial conditions. The potential $V(\phi)$ of the Higgs field is not known, and the various models for it have free parameters. The values of these parameters may determine whether the phase transition leads to immediate domain formation or to inflation. To chart the inflation-producing region of this parameter space, ABM numerically simulated the behavior of the ϕ field in an expanding homogeneous radiation-dominated FRW (flat, i.e., $k=0$) background spacetime.

We applied our code to the same problem. We stick to the model potentials used by ABM, and to their "quasi-

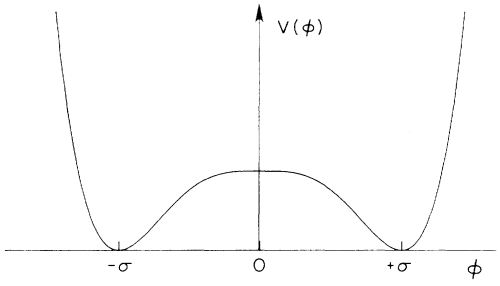

FIG. 4. The Coleman-Weinberg-type potential. The false vacuum corresponds to $\phi=0$ and the true vacua to $\phi=+\sigma$ and $\phi=-\sigma$.

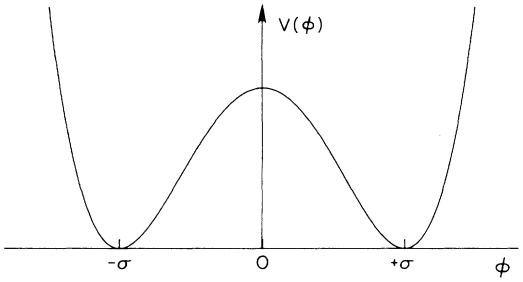

FIG. 5. The ϕ^4-type potential.

thermal" initial conditions, where the Higgs field is initially in the form of a standing plane wave. The potentials are a CW-type potential (Fig. 4)

$$V(\phi)=\lambda\phi^4\left[\ln\frac{\phi^2}{\sigma^2}-\frac{1}{2}\right]+\tfrac{1}{2}\lambda\sigma^4 \tag{4.1}$$

which, because of its central flatness, is ideal in producing the "slow rolling" of new inflation, and a simple double-well ϕ^4 potential (Fig. 5):

$$V(\phi)=\lambda(\phi-\sigma)^4 . \tag{4.2}$$

These models have two parameters: σ, the distance between the false and the true vacua, and λ, which is proportional to the energy density of the false vacuum ($\frac{1}{2}\lambda\sigma^4$ for the CW type, and $\lambda\sigma^4$ for the ϕ^4 type). Our third parameter will be the number $N-1$ of other particle species, whose contribution will be treated like a perfect fluid, assumed initially at rest with constant density.

We set our initial conditions at time t_0 to correspond to a temperature $T=\sigma$, so that the fluid has energy density

$$\rho_{(\text{fluid})}=(N-1)\frac{\pi^2}{30}T^4 . \tag{4.3}$$

The initial value for the scalar field is

$$\phi=B\cos kz,\quad \dot{\phi}=0 , \tag{4.4}$$

where $B=k=\sigma$, so that the initial fluctuations just reach the true vacua. This gives the scalar field an initial kinetic energy density $\frac{1}{2}B^2k^2\sin^2kz$, or $\frac{1}{4}B^2k^2=\frac{1}{4}T^4$ on average, close to $(\pi^2/30)T^4$, the contribution of one thermal mode.

In our code we use a grid of 50 zones with periodic boundary conditions to represent the z direction. We set the grid length equal to one wavelength, initially $L_w=2\pi/\sigma$. Assuming the expansion has been like $t^{1/2}$ until our initial time t_0, the horizon radius is then

$$L_H=2t_0=\frac{1}{H}=\left[\frac{3}{\rho}\right]^{1/2}=\left[\frac{90}{N\pi^2}\sigma^{-4}\right]^{1/2}\simeq\frac{3}{\sqrt{N}\,\sigma^2} . \tag{4.5}$$

Thus, the fraction of the initial horizon radius covered by our grid is

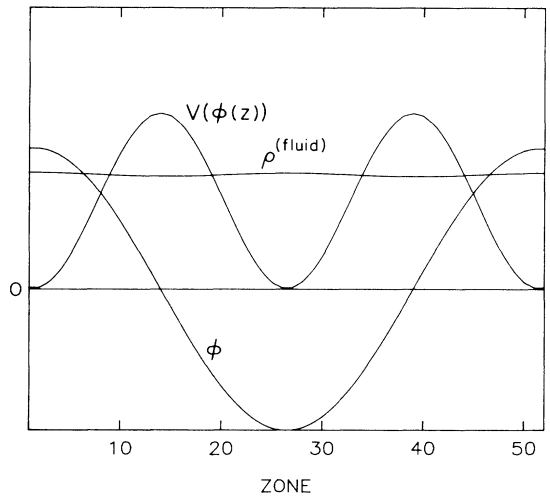

FIG. 6. Situation at the initial time. The scalar field ϕ has the form of a standing wave with amplitude σ. Its energy distribution is strongly inhomogeneous. The small inhomogeneity in the fluid density is produced by relaxing the initial data so that they satisfy the constraint equations.

$$\frac{L_w}{L_H}\simeq 2\sqrt{N}\,\sigma . \tag{4.6}$$

We did simulations with the parameters in the range

$$N=2,10 ,$$

$$\sigma=0.05,\ldots,0.5 ,$$

$$\lambda=10^{-4},\ldots,10^{-1} .$$

These values take us fairly close to the Planck time, which in our units is $t_{\text{Pl}}=1/\sqrt{8\pi}\simeq 0.20$. Our simulations have initial times from $t_0=1.9$ to $t_0=427$. We did not use smaller values of σ, because the computer time required for the simulation grows inversely proportional to σ.

We get the initial data for our simulation (see Fig. 6) by setting $\phi=\sigma\sin\sigma z$, $\dot{\phi}=0$, $D=0$, $E=(N-1)(\pi^2/30)\sigma^4$, $K_1=0$, $\beta^x=\beta^z=0$, $A=h=1$, corresponding to a flat three-space, and then relaxing it to satisfy the constraint equations. This typically produces a small β^z and a small inhomogeneity of the three-metric.

V. THE RESULTS OF SIMULATIONS

We do simulation runs with different values of the parameters λ, σ, N. We follow the simulation until one of two things happens: either ϕ falls down to the true vacuum completing the phase transition without inflation, or we enter an inflationary era where the Universe rapidly expands many orders of magnitude. In the latter case ϕ oscillations are frozen and ϕ soon becomes localized very close to the false vacuum.

The outcome is determined by the competition of two effects: the expansion of the Universe damps the ϕ oscillations and tends to localize ϕ close to its average value $\phi=0$, the false vacuum. On the other hand, the potential

pulls ϕ down towards the true vacua at $\phi=+\sigma$ and $\phi=-\sigma$. The damping also reduces the kinetic energy density of ϕ, weakening its ability to resist the pull of the potential.

The crucial time is when the vacuum energy density becomes equal to the radiation energy density. This happens close to the time

$$t\simeq\sqrt{3}N^{1/2}\lambda^{-1/2}t_0 \tag{5.1}$$

which is proportional to $\lambda^{-1/2}\sigma^{-2}$. The simulation time step is limited by the Courant condition to be smaller than the light travel time across a zone width, which we have set to $\frac{1}{50}$ of the ϕ oscillation wavelength, proportional to σ^{-1}. The number of time steps required in a simulation run is thus proportional to $\lambda^{-1/2}\sigma^{-1}$, making the computer time demand largest for small λ and σ.

In our runs the inhomogeneities in geometry or the fluid distribution typically do not grow large. Before the phase transition, the ϕ oscillations are being dampened and soon the smoothing effect of the overall expansion overrides any inhomogeneous effects of the scalar field. In the inflating runs the Universe soon becomes extremely homogeneous. In the noninflating runs we do see faster expansion in the regions where the ϕ energy is largest. This is reflected in the fluid density so that the fluid is most dense, where the expansion has been slowest. The fluid density contrasts reached in the noninflating run vary from below 1% to about 25%, the highest values obtained after domain formation. The produced fluid velocities remain nonrelativistic. The domain walls become too sharp (an extreme inhomogeneity in ϕ) for the code too soon for the effect of the wall on geometry to reach an interesting magnitude.

Thus, the interesting quantities are the ϕ field and the overall expansion. We found the best way to represent the ϕ behavior is to plot its minimum and maximum values. In the same plots we represent the expansion by

$$R=\left[\frac{V}{V_0}\right]^{1/3}, \tag{5.2}$$

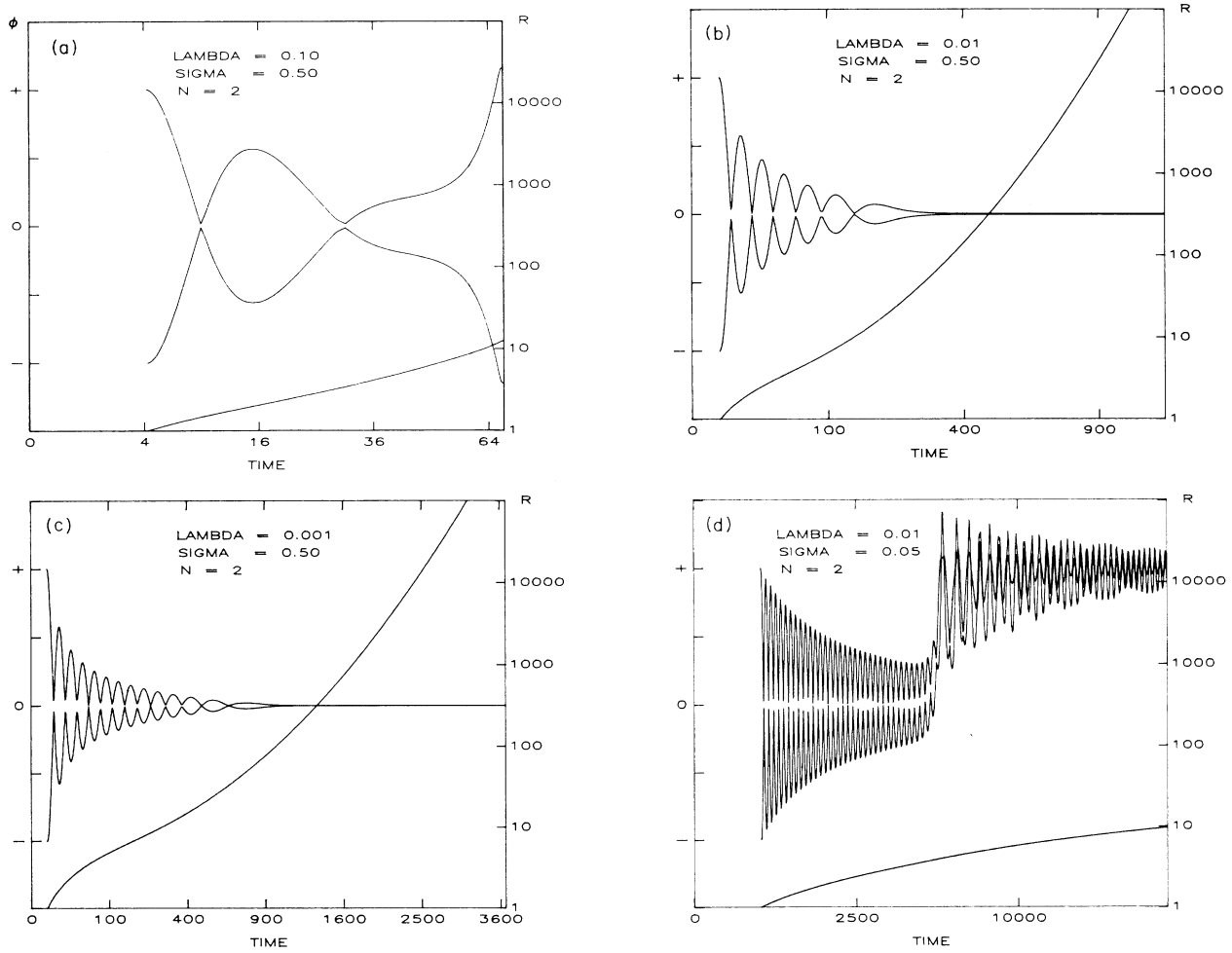

FIG. 7. Coleman-Weinberg potential runs with $N=2$. In these figures we plot the time evolution of the minimum and maximum values of the scalar field ϕ and the expansion factor R. The time axis is linear in $t^{1/2}$. The left vertical axis gives the ϕ scale, + and − marking the true vacua $+\sigma$ and $-\sigma$. (a) shows an almost immediate domain formation. (b), (c), and (g) are examples of inflation. (d), (e), and (f) show a phase transition without domain-wall formation.

where V/V_0 is the ratio of the volume of the space to its initial volume at t_0.

The time scale in the figures of the ϕ behavior refers to our time coordinate t, which is equal to the proper time measured by an observer located at the boundary of our grid. Observers located at other points of the grid measure slightly different proper times given by the lapse function α, which, however, is closely unity everywhere.

The first simulations are with the CW-type potential. Figure 7 shows runs with $N=2$. For a large λ, the vacuum energy becomes dominant soon, and we get almost immediate domain formation [Fig. 7(a) with $\lambda=0.1$ and $\sigma=0.50$]. In one-half of the grid ϕ falls to one of the true vacua $\phi=+\sigma$, and in the other to the other one, $\phi=-\sigma$. Thus, we get no inflation. For $\sigma=0.5$, smaller λ resulted in inflation. The ϕ oscillations are first damped by the expansion driven by the radiation energy density. When the vacuum energy density becomes dominant, ϕ is already localized to a region where the potential is too flat to be able to pull ϕ down. Instead the exponential expansion due to the vacuum energy damps ϕ further and soon it freezes it altogether. We see $\max|\phi|$ becoming very small and later beginning to grow extremely slowly.

At the end of the run $\lambda=10^{-2}$, $\sigma=0.5$, $N=2$ [Fig. 7(b)] at $t=1230$, the expansion factor is $R=0.8\times10^6$ growing exponentially with a doubling time $\Delta t\simeq60$, while $\max|\phi|$ is increasing at a rate $d\phi/dt\simeq10^{-7}\sigma$ without any detectable acceleration. With this rate the true vacuum would be reached when $R\sim10^{50\,000}$. With smaller λ the final $\max|\phi|$ and $d\max|\phi|/dt$ are even smaller.

Our code could not follow the inflation further than expansion factors in $R\sim10^6$. The reason is that we are rapidly approaching a pure de Sitter space where $(\mathrm{tr}K)^2=3\rho_{\mathrm{vac}}$. Because of the role played by $\mathrm{tr}K(t)$, "York time,"[7] in our code, the code cannot simulate a spacetime with $\partial_t(\mathrm{tr}K)=0$. Both the lapse equation and the Hamiltonian constraint have source terms that contain the difference $\frac{1}{3}(\mathrm{tr}K)^2-\rho_{\mathrm{vac}}$. This difference should gracefully approach zero. In our runs the two numbers typically become equal only up to eight digits, and their difference finally begins to dominate the source terms (all others going toward 0). This ruins the simulation. By

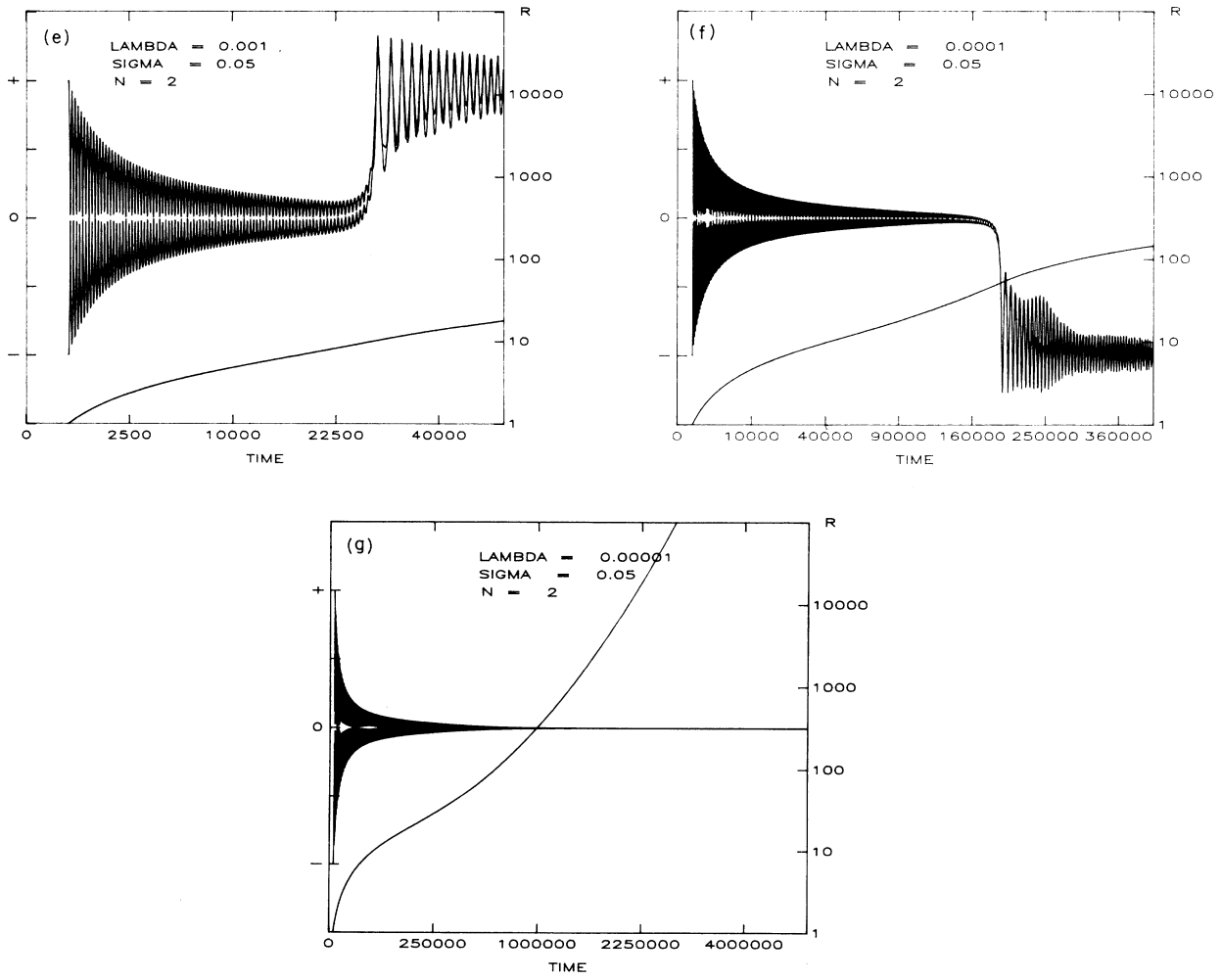

FIG. 7. (*Continued*).

this time we have typically reached a 10^5-fold expansion of the scale factor. Figure 7(c) shows a solution with $\sigma=0.5$ but smaller $\lambda,\lambda=10^{-3}$, which inflates after a longer period of oscillation than Fig. 7(b).

In simulations with $\sigma=0.05$, lowering λ to 10^{-2}, 10^{-3}, and 10^{-4} (Figs. 7(d), 7(e), and 7(f)] was not enough to produce inflation. Instead ϕ makes the transition to the true vacuum. The latent (vacuum) energy released in this transition is manifested in the large oscillations of ϕ around the new vacuum, which gradually damp in the continuing (noninflationary) expansion. Inflation was again realized for $\sigma=0.05$, $\lambda=10^{-5}$ [Fig. 7(g)].

We repeated these runs for $N=10$ and got very similar results. Because of the higher radiation energy density at a given temperature, the time scale is shortened. Otherwise there were few effects from changing N. For $\sigma=0.5$, $\lambda=0.001$ we get inflation like with $N=2$, but $N=10$, $\sigma=0.5$, $\lambda=0.01$ appears to be a marginal case. This run has a "mini-inflation," which at the end of the simulation is already showing signs of transition to the true vacuum (Fig. 8).

Figure 9 summarizes our results. They are in a qualitative agreement with ABM on the parameter region favorable for inflation. Quantitatively we find that the maximum λ to give inflation with a given σ is at least one order of magnitude smaller than ABM predict.

We also did some runs with the ϕ^4-type potential [Figs. (10a)—(10d)]. Because of the round shape of the potential, ϕ falls down easily, and this potential is not favorable for inflation. Indeed, we did not get inflation with any of the parameter values tried and the runs always ended with a phase transition (Fig. 11).

In some cases we see ϕ falling totally to one side, in others a domain wall forms separating two regions in the two different true vacua. This situation is partly an artifact of our setup and the prediction of the domain size is not to be taken seriously. We started with perfectly

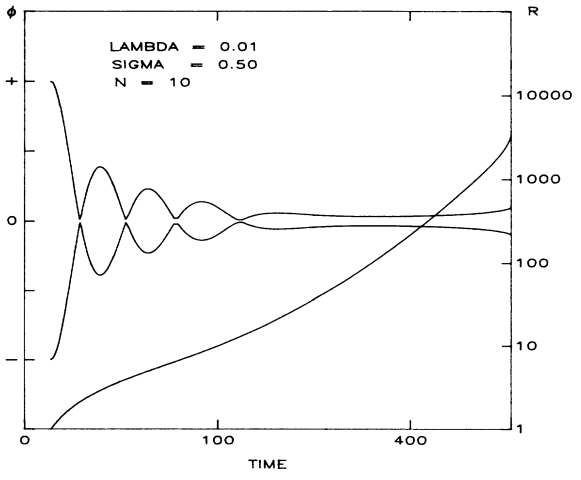

FIG. 8. A marginal case: "mini-inflation." The oscillation of the ϕ field is frozen and ϕ is localized near the false vacuum, but not well enough, so that after a short period of inflation it begins to fall towards the true vacua.

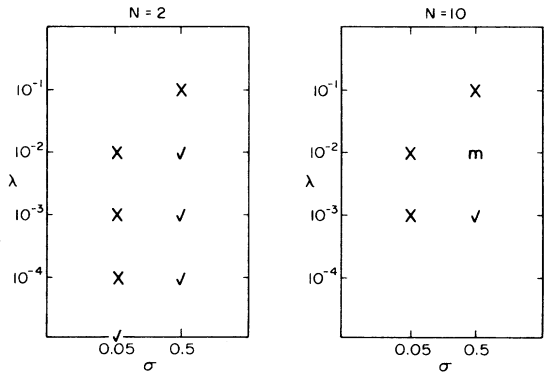

FIG. 9. Summary of the results with the CW-type potential. Checks mark runs that entered an inflationary era. Crosses mark runs that completed the phase transition without inflation. *m* marks a run with mini-inflation, a marginal case. In comparing with ABM, note that because of different units, our σ is $\sqrt{8\pi}\simeq 5.0$ times theirs.

symmetrical initial conditions. Conservation of this symmetry would prevent ϕ from falling totally to one side, so we could only form half-wavelength domains. That this is not always the case is due to a small asymmetry introduced by numerical errors. However, the *occurrence* of the phase transition is insensitive to these errors and is a reliable prediction of our simulation.

In reality the ϕ fluctuations would not have this perfect symmetry and we would get larger domains. To simulate this would require a larger grid (200—500 zones) to accommodate many wavelengths. Finer zoning (initially containing only one wavelength) would ameliorate the problem of continuing the evolution beyond domain formations (see Sec. VI).

Our code ran into stability problems when simulating domain walls. Sometimes this happened immediately when the domains formed, ending the simulation there, sometimes we were able to follow them for some time. One of the better cases is shown in Figs. 12 and 13 for a ϕ^4 potential. Because of the energy of the wall, spacetimes with domain walls expand faster than those in a single domain.

The main feature in our treatment is the gravitational effect of the scalar field. For comparison we did a few runs with ϕ terms eliminated from the gravitational source terms. [We compensated this by using $N(\pi^2/30)\sigma^4$ instead of $(N-1)(\pi^2/30)\sigma^4$ for the initial fluid energy density.] These have a homogeneous $R\propto t^{1/2}$ expansion due to the radiation fluid. Thus, the model becomes equivalent to that used by ABM. The results we get are now exactly the same as theirs. This serves as an additional test for our code. Figure 14 shows two example runs. Both of these are considered inflation producing by the criterion employed by ABM. That is, the equation of state becomes inflationary before the transition to the true vacuum takes place. The inflation is not actually seen here, because the effect of the scalar field on the geometry is now ignored.

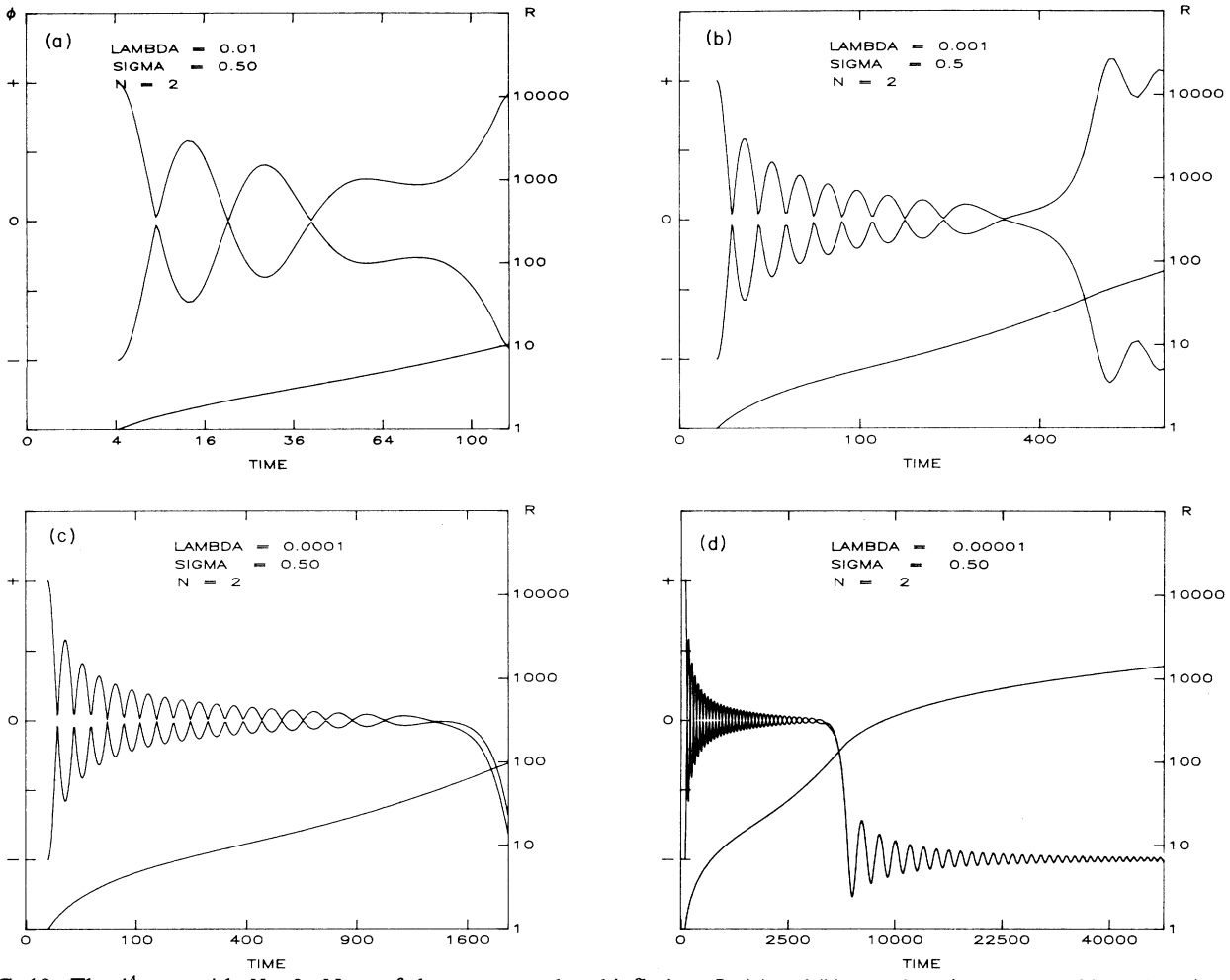

FIG. 10. The ϕ^4 runs with $N=2$. None of these runs produced inflation. In (a) and (b), two domains, separated by a domain wall, are formed. In (c) and (d), the ϕ field falls entirely to the $\phi=-\sigma$ vacuum.

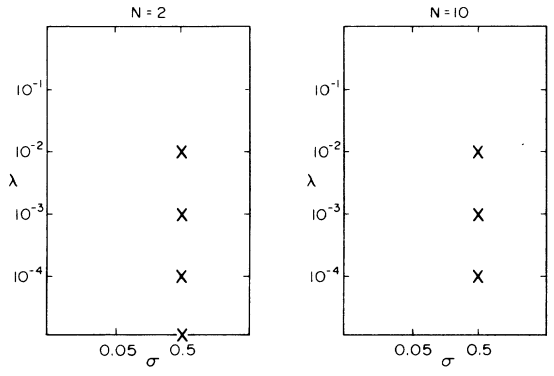

FIG. 11. Summary of the results with the ϕ^4-type potential. None of our simulations led to inflation.

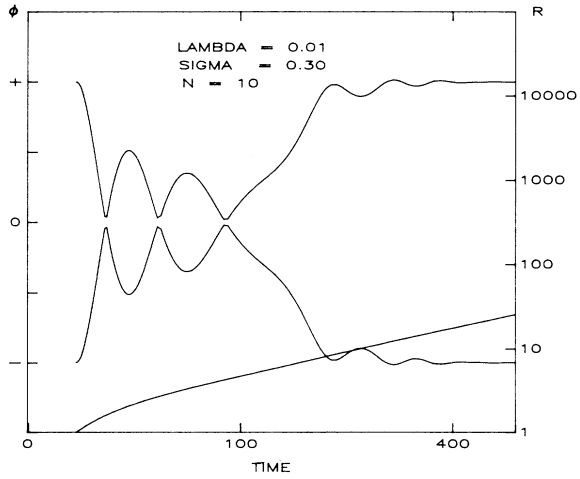

FIG. 12. Domain formation. Because of the energy in the domain walls a spacetime with domain walls expands faster after the phase transition than one without. Inside the domains the oscillations of the ϕ field are dampened by expansion. This simulation is for a ϕ^4-type potential with $\lambda=10^{-2}$, $\sigma=0.3$, and $N=10$.

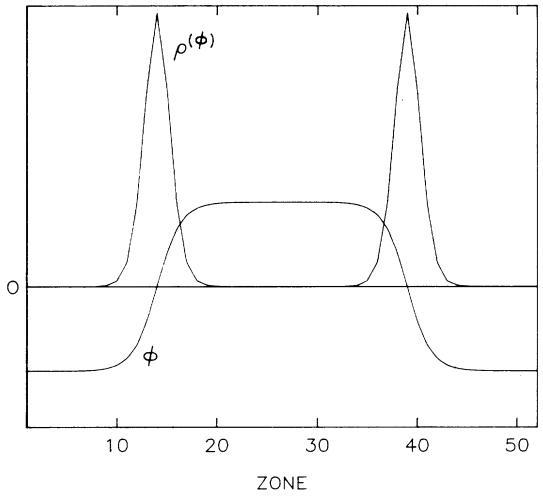

FIG. 13. Domain walls. The situation in the simulation of Fig. 12 at $t=520$. The energy content is dominated by the domain walls. The energy density of the fluid is too small to show in this scale.

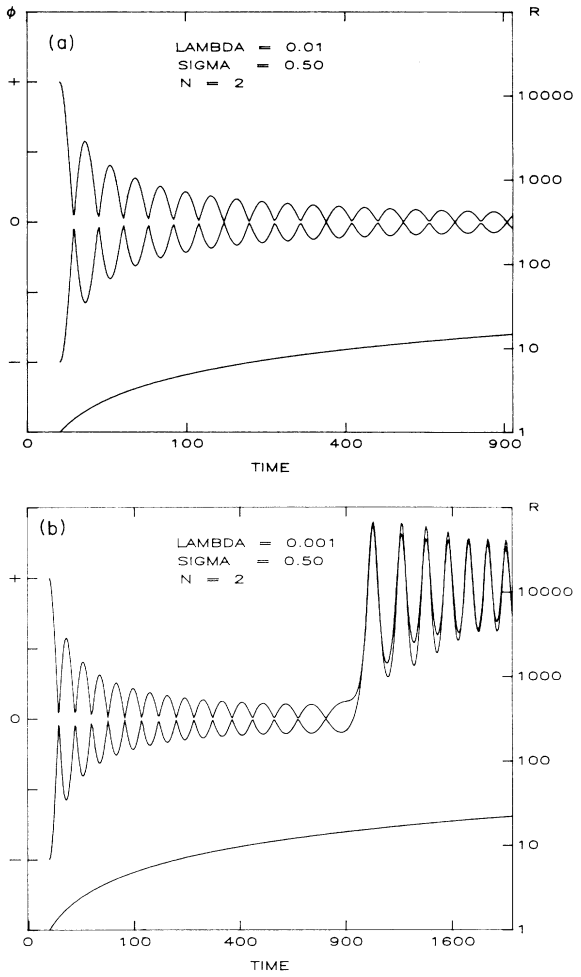

FIG. 14. Runs where the gravitational effect of the ϕ field is ignored. (a) A CW-type potential [compare to Fig. 7(b)]. No phase transition takes place and the ϕ oscillations are dampened and localized at the false vacuum. No inflation is seen because the vacuum energy is ignored by the gravitational equations. (b) A ϕ^4-type potential [compare to Fig. 10(b)]. Here we observe a phase transition. It happens later than in a full simulation, because without the vacuum energy contribution, the expansion and the resulting damping of oscillations are slower.

Comparing Figs. 14 to the runs done with the full model, we see that with the full model the transition to the true vacuum tends to happen earlier. This is because, as the expansion is becoming faster under the influence of the vacuum energy, ϕ is losing kinetic energy and cannot resist the pull toward the potential minima as well. Thus, our results show that inflation is somewhat harder to realize in the full model than ABM predict. For the ϕ^4-type potential this difference appears to be crucial, while for the CW type we only observe a shift in the region of parameter space favorable for inflation.

VI. CONCLUSIONS

We have written a fully general-relativistic computer code that simulates a plane-symmetric spacetime filled with a perfect fluid and a scalar field. To our knowledge this is the first time this kind of code has been written. We have used the code to simulate at the level of classical scalar field theory the phase transition of the new inflationary scenario with inhomogeneous initial data for the scalar field ϕ. Figure 15 shows the scalar field behavior in two typical runs: one (CW-type potential) that does lead to inflation, and one (ϕ^4 type) that does not.

Our results supplement those of ABM, who have charted the region of the parameter space for which they predict inflation. With a CW-type potential our simulations follow fairly well their predictions: We see inflation for small λ and large σ. For a ϕ^4-type potential none of our simulations entered an inflationary phase, although some of the parameter combinations were fairly deep inside the region for which ABM predict inflation.

The discrepancy arises because of an imprecise use of language by ABM. When they referred to inflation, they meant only that $p\sim-\rho$ for the ϕ-field quantities, without considering whether the ϕ-field contributions dominate as gravitational sources. Hence, a solution that approached $|\phi|\sim 0$ for an interval longer than several ϕ-oscillation periods was called "inflating" by ABM. If $\sigma \lesssim m_{\rm Pl}$, so that the ϕ field can truly be treated classically, such $|\phi|\sim 0$ states do not in fact last long enough when $V=\lambda(\phi^2-\sigma^2)^2$ to actually produce inflation in our back-reacting model.

It is a difficult task to write a stable and accurate code to handle the complicated combination of fluid, gravitation and scalar field dynamics involved. We found that the present code has certain limitations on what kind of simulations it can handle. Specifically, the emergence of domain walls or getting too close to a de Sitter spacetime eventually ruins a simulation. We emphasize that neither

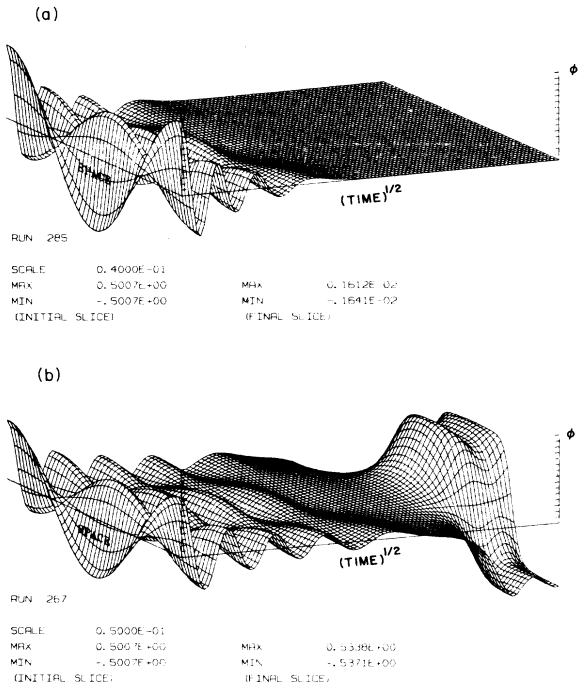

FIG. 15. Three-dimensional plots showing the evolution of ϕ on the entire grid. "Scale" refers to the tick interval on the vertical axis. (a) is from the same run as Fig. 7(b) and (b) is from the run of Fig. 10(b). In both cases the initial standing wave is first damped by the expansion. In (a) (CW-type potential) this prevents the phase transition, ϕ stays at the false vacuum and we get inflation. In (b) (ϕ^4-type potential) the phase transition takes place, two domain walls form, and inflation is prevented.

of these shortcomings of the code interferes with our determination of whether or not a particular set of initial data will produce inflation.

Solution of both these problems will require extensive modification of the code. Consider first the formation of the domain walls. The wall separates regions of inequivalent true vacuum. The field ϕ in the region of the wall possesses at the center of the wall potential energy equal to $V(0)$ ($=\lambda\sigma^4$ in a ϕ^4 model). This wall can be completely static because there is no energy profit by moving it to one side or the other (as there would be if the "vacua" on the two sides in fact had different energies). The thickness x of the wall is determined by minimizing the total energy in each surface element A of the wall. That arising from gradients of ϕ is

$$\sim(\sigma/x)^2(xA) ,$$

because the total excursion of the ϕ field values is of order σ in a distance x; this is multiplied by a volume element xA. The contribution from the potential is approximately

$$V(0)xA=\lambda\sigma^4(xA) .$$

Minimizing the potential contribution by making the thickness smaller increases the contribution from the gradients. The minimum energy per unit area in the wall is found to occur when

$$x\sim\sigma\lambda^{-1/2} .$$

For our simulations, it is relevant to compare this to the size of our grid: initially the proper length of our grid is (see Sec. IV)

$$L_w=\frac{2\pi}{\sigma} ;$$

then, initially

$$x/L_w=\frac{1}{2\pi}\frac{1}{\lambda^{1/2}} .$$

One of our typical runs that forms domains [Fig. 7(a)] has $\lambda^{1/2}=0.32$. So $x/L_w\sim 0.5$ initially. However, quantities involving the parameters of the potential are given by microphysics and are independent of the expansion of the Universe, while the grid size is comoving. Hence, at a later time

$$x/L_w\simeq\frac{1}{2\pi}\lambda^{-1/2}R^{-1} ,$$

assuming R normalized to unity initially. We can expect difficulty when the wall thickness approaches one zone. The final points plotted in Fig. 7(a) have $R\sim 15$; thus $x/L_w\simeq\frac{1}{30}$. This is consistent with our 50-zone grid; the code crashes when the wall thickness $\sim$ one zone. We see that direct computation through domain formation by actually resolving the wall requires an increasingly fine grid to further extend the evolution. Although this can be initially successful, long evolution will demand an impractically finely divided grid. Other methods especially adapted to handling large discontinuities will have to be employed. Because of the static nature of the walls, usual "artificial viscosity" procedures, which depend on time dependence of the fields, are inapplicable here.

Attempting to make the code follow closely de Sitter cosmologies will also demand extensive revision. A different time-slicing algorithm (in other words, a different gauge choice for the time) must be introduced, since it is the inability of the code to distinguish different three-spaces with almost identical extrinsic curvature tr$K$ (in the de Sitter case, tr$K$ is identically constant) that causes the failure. Perhaps a change to three-volume as coordinate time, or to proper time, will be needed. It remains to be seen whether we can improve the code to handle these cases. It would be exciting if we could follow a simulation well past domain formation, or could evolve the inflation all the way through until reheating.

We have also begun simulations which use an old-inflationary-type potential that leads to formation of bubbles. In this case the bubbles are dynamic and it is possible to introduce a coupling between ϕ and the fluid to keep the bubble surface at finite thickness. This will be the subject of a future paper.

ACKNOWLEDGMENTS

We thank Andreas Albrecht, Robert Brandenberger, Paul Steinhardt, and J. M. Yuan for very useful discussions. H. Kurki-Suonio gratefully acknowledges financial support from the Henny and Antti Wihuri Foundation and the Academy of Finland. This work was supported in part by NSF Grants Nos. PHY84-04931, PHY84-17918, and PHY84-51732 and by Lawrence Livermore National Laboratory under DOE Contract No. W-7405-ENG-48.

---

[1]A. Guth, Phys. Rev. D **23**, 347 (1981); A. Linde, Phys. Lett. **108B**, 389 (1982); A. Albrecht and P. Steinhardt, Phys. Rev. Lett. **48**, 1220 (1982); A. Linde, Rep. Prog. Phys. **47**, 925 (1984); A. Albrecht, in *Fifth Workshop on Grand Unification,* edited by K. Kang, H. Fried, and P. Frampton (World Scientific, Singapore, 1984); R. Brandenberger, Rev. Mod. Phys. **57**, 1 (1985).

[2]G. Mazenko, W. Unruh, and R. Wald, Phys. Rev. D **31**, 273 (1985).

[3]S. Coleman and E. Weinberg, Phys. Rev. D **7**, 1880 (1973).

[4]R. Matzner, in proceedings of the Drexel Workshop on Numerical Relativity, edited by J. Centrella (unpublished).

[5]A. Albrecht, R. Brandenberger, and R. Matzner, Phys. Rev. D **32**, 1280 (1985); preceding paper, **35**, 429 (1987).

[6]J. Centrella and J. Wilson, Astrophys. J. **273**, 428 (1983); Astrophys. J. Suppl. **54**, 229 (1984).

[7]J. York, Phys. Rev. Lett. **28**, 1082 (1972).